A numerical model for delamination growth simulation in non-crimp fabric composites

Aniello Riccio, M. Zarrelli, N. Tessitore

A numerical model for delamination growth simulation in non-crimp fabric composites

Aniello Riccio, M. Zarrelli, N. Tessitore

PII: S0266-3538(07)00133-9
DOI: 10.1016/j.compscitech.2007.03.029
Reference: CSTE 3644

To appear in: *Composites Science and Technology*

Received Date: 31 July 2006
Revised Date: 19 March 2007
Accepted Date: 21 March 2007

Please cite this article as: Riccio, A., Zarrelli, M., Tessitore, N., A numerical model for delamination growth simulation in non-crimp fabric composites, *Composites Science and Technology* (2007), doi: 10.1016/j.compscitech.2007.03.029

A NUMERICAL MODEL FOR DELAMINATION GROWTH SIMULATION IN NON-CRIMP FABRIC COMPOSITES

Aniello Riccio[+], M. Zarrelli[*] and N.Tessitore[+]

[+]C.I.R.A - Italian Aerospace Research Centre, Via Maiorise, Capua, Caserta 81043 Italy

[*]CNR-Research National Council, IMCB – Inst. of Comp. and Biom. Mat., P. E. Fermi, Granatello, 80055 Portici (Na)

ABSTRACT

In this paper, a novel finite element tool, for the simulation of delamination growth in Non-Crimp fabric (NCF) composite materials, is presented. The proposed finite element tool is based on the Stiffness Averaging Method (SAM), on the Modified Virtual Crack Closure Technique (MVCCT) and on the Penalty Method (PM); all these methods have been implemented in the research oriented B2000 Finite Element code. The Stiffness Averaging Method allows taking into account the effects of the processing variables, which characterize the Representative Volume Element (RVE) of the Non-Crimp Fiber composites (NCF) on their mechanical performances; while the Modified Virtual Crack Closure Technique is used to determine the Strain Energy Release Rate (SERR) for the delamination growth. Already available experimental data on Mode I fracture toughness, obtained by using Double Cantilever Beam (DCB) tests have been employed for validation purpose of numerical procedure. The modeling of DCB tests, considering different geometrical cases, has been performed by means of non-linear analyses. Excellent results in terms of deformed shapes and load-displacement curve, compared with experimental data, are reported to support the validity and the accuracy of the presented computational procedure. Moreover, the ability of the developed tool to take account for the NCF performances variability with processing parameters along with the delamination growth has been assessed and critically discussed.

Keywords: Textile composite (A), Modeling (B), Delamination (C), Finite Element Analisys (C).

1.0 INTRODUCTION

Composite materials are rapidly evolving from secondary non-load bearing applications to primary load bearing structural applications. In order to meet the consequent increased requirements, a significant improvement in the damage tolerance and reliability of these materials is needed as well as a reduction

in the costs related to their manufacturing. Traditional aerospace high-performance composites, based on unidirectional pre-preg tape, generally provide unsurpassed in-plane specific properties, but their manufacturing costs are still very high. Indeed, the material itself is expensive, as well as the time consuming lay-up process and the equipment needed for storage and cure. Moreover, the out-of-plane properties of traditional composites are usually low due to the lack of through-thickness reinforcements.

On the other hand, textile technology, in combination with liquid molding technique (RTM, RFI, etc.) offers economically attractive alternatives to the traditional pre-preg composites. Several different types of preforms are available, such as weaves, braided and knitted fabric. However, the amount of crimp present in the fiber yarns, although gains the integrity of the fabric, can cause a reduction of the in-plane material properties and can also induce dangerous failure mechanism (as kinkband formation). As a result, the Non-Crimp Fabrics based composites have attracted the attention of many researchers and industries, offering lower operating costs and improved through-thickness properties with no significant drop in the in-plane performances (indeed, the presence of the stitching threads between the fibre tows may give a benefit in terms of out-of-plane properties). Due to the complex architecture of NCF materials, the local geometrical and material characteristics can significantly influence the global mechanical properties. Thus, according to most of bibliographic sources, the preferred way to obtain an accurate global model is to first undertake the development of an accurate local model based on experimental and analytical consideration taking into account the micro-structure and the meso-structure of these innovative materials. An experimental investigation on the NCF composites is performed in [1] where a comparison with standard tape composites is carried out highlighting the improved performances of NCFs in terms of compression after impact strength and the limited loss in terms of compression and tension strength with respect to tape laminates.

The influence of stacking sequence on the NCF elastic properties has been experimentally investigated in [2] where the results of tension tests on multilayered warp-knit fabric reinforced epoxy composites with different material lay-ups are presented and discussed. In [3] a review of the main analytical models for the prediction of thermo elastic properties of two- and three-dimensional fabrics is presented. Several analytical models can be found in literature, which are based on assumptions on the geometric and

mechanics characteristics of NCF composites constituents. In [4] the stiffness averaging method is introduced and applied to multi-axial warp-knit fabrics; a relevant improvement in the industrial design process involving such materials is demonstrated. References [5] and [6] present two-dimensional models for biaxial fabrics able to relate respectively the NCF compressive and shear properties to the geometrical and mechanics characteristics of the constituents; however the validity of these models is limited to specific loading conditions. In [7] a basic analytical model based on the rule of mixture for determining the tensile elastic modulus of knitted fabric reinforced epoxy laminates is introduced; the validation of this model is justified in [8] where a relevant experimental campaign on NCFs is reported and discussed. In [9] the "cross over model" is presented underlining its ability to determine the elastic properties of the NCF composites by averaging the properties of the constituent curved yarns and its limitation for composites with high volumetric fraction of fibers. In [10] three analytical simplified models: the "mosaic model" the "fiber undulation model" and the "bridging model" for determining the stiffness and the strength behavior of woven fabrics are presented; these models are shown to be effective only for non-braided composites. Reference [11] introduces an approximated analytical model for NCF composites elastic properties evaluation based on the Timoshenko beam theory; the model validation by comparisons with experimental results, is carried out for cross-ply laminates under tensile load. In [12] the "fabric geometric model" able to relate the fibre architecture and the material properties to the global stiffens properties of textile reinforced composites is analyzed and its limitations in terms of matrices transformations and yarn modeling are discussed. Indeed, at micro-scale level the fibre-matrix structure within the tows needs to be taken into account by means of a micro-mechanical approach in order to correctly consider the load transfer between fibres and matrix. At meso-scale level (preform level) the defects in the NCFs (as, for example, the waviness of the tows) need to be considered in order to set up a realistic three-dimensional effective model for the determination of the mechanical performances of the NCFs. The failure mechanisms and the fracture toughness properties are also influenced by the micro-structure and the meso-structure of the NCFs as shown in [13,14], where the formation of damage and its progression are investigated by fractography and the influence of stitching on NCFs toughness properties is assessed by experimental tests [15,16]. Very few examples of failure

analytical models can be found in literature. In [17] an analytical model based on the "fracture surface approach" is introduced to simulate the failure behavior of NCFs. A good agreement has been found with experimental data but only for plain stitch fabric composites. Hence new analytical more general failure models able to take into account the important aspects related to micro-structure and meso-structure of the NCFs are needed in order to correctly predict the damage propagation and in particular the delamination growth under generic loading conditions.

This paper presents a novel finite element based approach able to represent the complex architecture of the Non-Crimp Fabric composite materials and to simulate their mechanical behavior. By means of the Stiffness Averaging Method [4,12], the proposed model, derived by a previously developed method [18], takes into account the processing variables (fibres and matrix components, type of stitching, type of dry preform, fibre waviness, stitching parameters, etc.) affecting the mechanical performances within a defined Representative Volume Element. The damage progression in terms of delamination growth has been simulated by interface elements based on the Modified Virtual Crack Closure Technique [19] for the evaluation of the Strain Energy Release Rate contributions. The proposed FEM approach has been implemented in the finite element code "research oriented" B2000 and validated by means of comparisons with experimental data on delaminated Double Cantilever Beam coupons. Different coupons configurations characterized by different geometrical parameters (stitch length, stitch gauge) and different processing technique (Resin Film Infusion – RFI- and Resin Infusion under Flexible Tooling – RIFT) have been analyzed, in order to investigate the capability of the developed tool to take into account the relative changes in mechanical performances including delamination growth. In the following sections, the theoretical background of the implemented approach and the numerical applications will be described. First of all, the theory behind the Representative Volume Evaluation approach and the Stiffness Averaging Method implementation is introduced. The Modified Virtual Crack Closure Technique will be also described in details. Then, the comparisons between the obtained numerical results and experimental data for the Double Cantilever Beam (DCB) coupons will be presented, in order to validate the proposed FEM tool for different configurations in terms of deformed

shapes and load-displacement curves. Finally the influence of the geometrical and processing parameters on the mechanical behavior and delamination growth will be discussed and critically assessed.

2.0 THEORETICAL BACKGROUND

In this section, the theory underlying the NCF material formulation and the delamination growth model are presented. Hereafter, the definition of the RVE along with description and implementation of the Stiffness Averaging Method for modelling the complex architecture of the textile RVE, are extensively explained. Furthermore, the detailed description of the NCF composites delamination growth model is given.

2.1 INSIGHT OF ASSUMED REPETITIVE VOLUME ELEMENT (RVE)

The Repetitive Volume Element can be defined as the smallest repetitive portion of the material whose properties are representative of the global mechanical performance of the NCF. The geometric definition of the RVE is based on the following processing parameters (see figures 1 and 2):

S_{len} = stitch length; n_{ax} = number of tows along the thickness in the preform;

S_{gauge} = stitch gauge; a_1, a_2= thicknesses of the tow

θ_{stitch} = stitch angle;

The RVE of a biaxial NCF preform with a chain stitched pattern is shown in figure 1. The geometry of RVE depends on the processing parameters as follows:

$$\mathrm{H}_{cell} = a_1 + a_2 \; ; L_{cell} = \frac{S_{len}}{\cos(\theta_{stitch})} \; ; W_{cell} = \cos(\theta_{stitch}) \cdot S_{gauge} \tag{1}$$

The individual tows of the NCF can be slightly wavy. With reference to figure 2, in order to take into account the tows' waviness from a modeling point of view, it is possible to assume a sinusoidal function to model their out of plane directional path [11]. Thus, we can write the equation representing the middle line of the tow:

$$z(x) = \left(a_1 + \frac{a_2}{2} - \frac{c}{2} \right) \cdot \cos\left(\frac{2\pi x}{\lambda} \right) \tag{2}$$

where a_1 and a_2 are the tows' thickness, λ is the wavelength, $c/2$ is the wave amplitude, z and x are the coordinates in the plane $y=0$ of the RVE reference system. The amplitude is experimentally determined from the measured Standard Deviation of Orientation (SDO) of the tows. A cosine function has been found to be rather representative of the shape of these waves [20,21]. The so defined RVE is applicable for every loading condition. However, this approach is not able to take into account the stitching tension within the RVE definition.

2.2 STIFFNESS AVERAGING APPROACH

The contribution of each NCF component (tows, stitching threads) over the total RVE stiffness has been calculated by means of the Stiffness Averaging Method. One attractive feature of this method is that, although continuity of internal stresses is violated, continuity of strains (and thus displacements) is maintained. From a mechanical point of view, due to the high non-homogeneity of the RVE components, a reduced level of approximation is expected if the continuity of displacement rather then stress is assumed. The proposed approach is based on the subdivision of the reinforcement and tows systems of the RVE into distinct sets of sub-volumes respectively able to follow the path of the stitching thread and the path of the tows' waviness. Each sub-volume is considered made of fibres correctly oriented and surrounded by the matrix. In figure 3 the stitching and the tow sub-volumes are schematically shown. Being each sub-volume made of fibers and matrix, it is possible to find the engineering constants representing its performances by means of the micromechanical theories based rules of mixture [7] which can give the properties of each sub-volume as a function of the properties of the constituents and of their volumetric fractions.

In case of rich resin regions, the resin is associated to the closest sub-volume (i.e. stitching sub-volume or tow sub-volume). Furthermore, the sub-volumes are assumed not interacting each other, and the RVE of the NCF composite can be considered as subjected to a constant strain state. For each sub-volume, a local reference system is introduced with x-axis in the fiber direction and y-axis and z-axis normal to the fiber direction (see figure 3). Under these assumptions, the material in the RVE can be considered transversely isotropic with respect to x-axis direction. From the transversely isotropic engineering

constants of the i^{th} sub-volumes it is possible to write its material stiffness matrix, in the local reference system, as:

$$C_{loc}^{i}=\begin{bmatrix} C_{11} & C_{12} & C_{12} & 0 & 0 & 0 \\ C_{12} & C_{22} & C_{23} & 0 & 0 & 0 \\ C_{12} & C_{23} & C_{33} & 0 & 0 & 0 \\ 0 & 0 & 0 & C_{44} & 0 & 0 \\ 0 & 0 & 0 & 0 & (C_{22}-C_{23})/2 & 0 \\ 0 & 0 & 0 & 0 & 0 & C_{44} \end{bmatrix} \tag{3}$$

with

$$\begin{aligned} &C_{11}=\frac{1-\nu_{23}\nu_{32}}{\Delta E_2 E_3}, \mathrm{C}_{12}=\frac{\nu_{21}+\nu_{31}\nu_{23}}{\Delta E_2 E_3}, C_{22}=\frac{1-\nu_{13}\nu_{31}}{\Delta E_1 E_3} \\ &\mathrm{C}_{23}=\frac{\nu_{32}+\nu_{12}\nu_{31}}{\Delta E_1 E_3}, C_{55}=G_{23}=\frac{E_2}{2(1+\nu_{23})}=\frac{C_{22}-C_{23}}{2} \\ &C_{44}=G_{31}=G_{12} \\ &\Delta=\frac{1-\nu_{12}\nu_{21}-\nu_{23}\nu_{32}-\nu_{13}\nu_{31}-2\nu_{21}\nu_{32}\nu_{13}}{E_1 E_2 E_3} \end{aligned} \tag{4}$$

Then, the stiffness matrix of the i^{th} sub-volume, calculated in the local reference system, can be written in the RVE reference system by means of the transformation matrix T:

$$C_{RVE}^{i}=T^{i^T}\cdot C_{loc}^{i}\cdot T^{i} \tag{5}$$

with

$$T^{i}=\begin{bmatrix} {}^{i}l_1^2 & {}^{i}m_1^2 & {}^{i}n_1^2 & {}^{i}l_1{}^{i}m_1 & {}^{i}m_1{}^{i}n_1 & {}^{i}n_1{}^{i}l_1 \\ {}^{i}l_2^2 & {}^{i}m_2^2 & {}^{i}n_2^2 & {}^{i}l_2{}^{i}m_2 & {}^{i}m_2{}^{i}n_2 & {}^{i}n_2{}^{i}l_2 \\ {}^{i}l_3^2 & {}^{i}m_3^2 & {}^{i}n_3^2 & {}^{i}l_3{}^{i}m_3 & {}^{i}m_3{}^{i}n_3 & {}^{i}n_3{}^{i}l_3 \\ 2{}^{i}l_1{}^{i}l_2 & 2{}^{i}m_1{}^{i}m_2 & 2{}^{i}n_1{}^{i}n_2 & {}^{i}l_1{}^{i}m_2+{}^{i}l_2{}^{i}m_1 & {}^{i}m_1{}^{i}n_2+{}^{i}m_2{}^{i}n_1 & {}^{i}n_1{}^{i}l_2+{}^{i}n_2{}^{i}l_1 \\ 2{}^{i}l_2{}^{i}l_3 & 2{}^{i}m_2{}^{i}m_3 & 2{}^{i}n_2{}^{i}n_3 & {}^{i}l_2{}^{i}m_3+{}^{i}l_3{}^{i}m_2 & {}^{i}m_2{}^{i}n_3+{}^{i}m_3{}^{i}n_2 & {}^{i}n_2{}^{i}l_3+{}^{i}n_3{}^{i}l_2 \\ 2{}^{i}l_3{}^{i}l_1 & 2{}^{i}m_3{}^{i}m_1 & 2{}^{i}n_3{}^{i}n_1 & {}^{i}l_3{}^{i}m_1+{}^{i}l_1{}^{i}m_3 & {}^{i}m_3{}^{i}n_1+{}^{i}m_1{}^{i}n_3 & {}^{i}n_3{}^{i}l_1+{}^{i}n_1{}^{i}l_3 \end{bmatrix} \tag{6}$$

where ${}^{i}l_j$, ${}^{i}m_j$, ${}^{i}n_j$ are the direction cosines of the i[th] local reference system in the RVE local coordinate system:

$$\begin{aligned} &{}^{i}l_1=\cos(x_{loc}^{i},x);\ {}^{i}m_1=\cos(y_{loc}^{i},x);\ {}^{i}n_1=\cos(z_{loc}^{i},x) \\ &{}^{i}l_2=\cos(x_{loc}^{i},y);\ {}^{i}m_2=\cos(y_{loc}^{i},y);\ {}^{i}n_2=\cos(z_{loc}^{i},y) \\ &{}^{i}l_3=\cos(x_{loc}^{i},z);\ {}^{i}m_3=\cos(y_{loc}^{i},z);\ {}^{i}n_3=\cos(z_{loc}^{i},z) \end{aligned} \tag{7}$$

The resulting stiffness of the stitching and tow sub-volumes can be calculated as:

$$C_{RVE} = \sum_{i=1}^{n_{st}+n_{tow}} \left[k^i \cdot C^i_{RVE} \right] \tag{8}$$

where n_{st} and n_{tow} are respectively the total number of sub-volumes for the stitching and the tows in the RVE. $k^i = \dfrac{A^i \cdot L^i}{V_{tot}}$ is the volumetric fraction of the i^{th} sub-volume with respect to the total volume V_{tot} of the RVE (A_i and L_i being respectively the cross section area and the length of the i^{th} sub-volume). Using equation (7), the mechanical behavior of the RVE and hence, the material properties of the NCFs are fully characterized.

2.3 DELAMINATION GROWTH IMPLEMENTATION

Delaminations in NCF fabric composite materials, as well as in the standard laminated composites, can rise up during the manufacturing process or they can arise as a consequence of impacts with foreign objects. Whatever is the mechanism, in some cases, delaminations can result very dangerous for the whole composite structure as they can lead to an abruptly and premature collapse. In the NCFs, the delamination on-set and growth can be strongly influenced by the knitting and the stitching [8,9,15,16].

Within the frame of EU project, FALCOM, a numerical tool has been developed to simulate the delamination propagation in NCF composites. The implemented numerical procedure has been used to investigate in details the influence of this damage mechanism on the load-carrying capability of the composite panels finding very comfortable result with experiments comparison. From fracture mechanics, it is well known that Strain Energy Release Rate drives the propagation of cracks. Thus for each fracture mode (opening Mode I, forward shear Mode II and parallel shear Mode III) a strain energy release rate can be defined: G_I for mode I, G_{II} for mode II and G_{III} for mode III. Once known, from ad hoc experiments, the critical energy release rates for the basic fracture modes (G_{IC}, G_{IIC} and G_{IIIC}), it is possible to predict the crack propagation by adopting suitable criteria such as the power law criterion. For the application of interest, only the mode I has been considered and the following criterion has been applied:

$$\left(\frac{G_I}{G_{I_C}} \right)^{\alpha} = E_d \geq 1 \tag{9}$$

Indeed, a linear criterion has been applied by setting α equal to 1. The satisfaction of relation (8) is assumed to be the necessary condition for crack propagation. In order to adapt the delamination growth procedure, successfully tested for laminated composites, to NCFs, the critical SERR values need to be experimentally evaluated for the NCF composite materials under investigation.

It is worth to assume that the critical values of SERR, obtained experimentally, would take into account the influence of knitting and stitching on the delamination growth. The delamination growth procedure has been implemented in our FE code by means of a new 9-noded interface fracture element. This element encodes the Modified Virtual Crack Closure Technique (MVCCT), presented in [19], to calculate the SERR on the delamination front. The standard VCCT is based on the assumption that the Strain Energy released by a single crack growing in length from a to $a+\Delta a$ is equal to the amount of the work required to close the same crack from $a+\Delta a$ to a. Thus, the implementation of such a method allows calculating the Strain Energy Released as a crack closure work but it involves two analyses; the first with the current crack front and the other with the crack front appropriately extended. On the other hand, the MVCCT, which - like the VCCT - is still based on the $\Delta a/a << 1$ hypothesis, assumes that, since the crack front does not undergo substantial changes in the evolution from the crack length a to $a+\Delta a$, the second step calculations (with extended crack configuration) can be avoided. Indeed it is possible to compute the SERR contributions in one step by using nodal forces and displacements estimated at the actual crack front. The interface fracture elements are placed between the solid elements with the nodes rigidly connected to the nodes of the adjacent solid elements. The Unit Virtual Crack Closure Work, which is equal to the Strain Energy Release Rate, for each fracture mode can be computed using nodal forces and nodal displacements calculated at the delamination front. For example, the mode I Strain Energy Release Rate, associated to the interface fracture element shown in figure 4, calculated in the node H can be written as:

$$G_I^H = \frac{1}{2}\cdot\frac{1}{(A_1+A_2)/2}\cdot F_n^H\cdot\left(u_n^M - u_n^L\right) \tag{10}$$

Where, A_1 and A_2 gives a measure of the area surrounding the node H, F_n^H is the normal component of the force in the node H, u_n^M and u_n^L represent respectively the displacement of the node M and L in the

normal direction. The interface fracture element local co-ordinate system (t,s,n), shown in figure 4.a, is used to take into account the large rotations of the delamination front for the calculation of fracture modes contributions and contact forces during growth. Introducing the computed values of: G_I, in the power law criterion (eq. 8) it is possible to check whether the propagation occurs. For the interface fracture element of figure 4, the satisfaction of the power law criterion leads to the release of the node H (see figure 4.b) that causes a modification in the delamination front. This kind of technique has been adopted in conjunction with the NCF finite-element in order to simulate the delamination growth in NCF composites.

2.4 EXPERIMENTAL REFERENCES FOR MATERIALS AND METHODS

Different RFI material configurations, namely, "long stitch", "2.5 mm gauge width" and "base" configurations (differing only in processing parameters S_{len} and S_{gauge}) have been analyzed to investigate the capability of presented numerical tool to take into account the influence of processing parameters on fracture toughness. The "base" configuration is characterized by the processing parameters S_{len} = 2.5 mm and S_{gauge} = 1.5 mm, the "long stitch" configuration is characterized by the processing parameters S_{len} = 4 mm and S_{gauge} = 4 mm and the "2.5 mm gauge width" configuration is characterized by the processing parameters S_{len} = 4 mm and S_{gauge} = 2.5 mm. Also the influence of the manufacturing process on the overall structural behavior of the DCB specimens has been considered by thoroughly analyzing a RIFT "long stitch" configuration (characterized by the processing parameters S_{len} = 4 mm and S_{gauge} = 4 mm). The analyzed RFI configurations are characterized by different processing parameters then, according to sections 2.1, they are characterized by Repetitive Volume Elements with different geometries. A schematic representation of the RVEs (with relevant dimensions) chosen for the RFI configurations is given in figure 5. As remarked in section 2.2, differences in RVE geometries imply differences in the material properties of the RVEs calculated by the Stiffness Averaging Method and then in the mechanical performances of the Non.Crimp Fabric. The RVEs chosen for the "long stitch" RFI and "long stitch" RIFT configurations have the same geometry; however differences in performances are expected due to the different material properties of the resin between these two configurations.

The geometrical description and the boundary conditions of the DCB test-cases are shown in figure 6. The DCB specimens stacking sequence was $[(90°/0°)_4]_s$ for the RFI and $[(90°/0°)_3]_s$ for the RIFT. All samples were cut off in the appropriate dimensions from composite plates and manufactured according to the processing conditions specified in [21,22]. Tow, type Tenax HTS carbon fibre 5632 12k, matrix resin M36 for RFI and RTM6 for RTM by Hexcel and the chain stitch, type Sinterama Zerbion -50 dtex-polyester, specified in [22,23], have been used. The tows and the matrix characteristics are summarized, respectively, in tables 1, 2, and 3. Where E and G are respectively, the Young and shear modulus; ν is the Poisson's ratio and V_m is the matrix volumetric fraction. Table 3 reports the stitching thread properties and geometrical characteristics; where E_1, E_2 and E_3 indicate, respectively, the longitudinal and transversal Young's moduli; $G_{12} = G_{13} = G_{23}$ are shear moduli; $\nu_{12} = \nu_{13} = \nu_{23}$ are Poisson's ratios; A, S_{gauge} and S_{len} represent, respectively the stitch area, the distance between stitching rows and the length of a stitch. In table 4 the experimentally determined mode I Critical Energy Release Rate G_{Ic} are shown for all the analyzed configurations.

3.0 NUMERICAL RESULTS

In order to validate and to assess the potential and the accuracy of the proposed numerical tool, some computational applications are presented hereafter. Analyses on different Double Cantilever Beam configurations of composite material samples have been performed in order to validate both the NCF material approach and the delamination growth approach. Numerical results have been also compared with experimental data of G_{Ic} obtained within the framework of the EU project, FALCOM, on the same configuration of tested specimens [22].

3.1 RFI BASE CONFIGURATION

Figure 7 shows the deformed shapes with an amplification factor of 5, at different steps during the loading process, for an RFI "base" configuration DCB tested sample. The growth of the delamination is clearly visible. In figure 8 the numerical load/applied displacement curve is compared with experimental data as available in the FALCOM project [22]. From the beginning of the loading process up to an applied displacement of 3.5 mm, the agreement between the numerical analysis and tests is excellent.

Beyond this point the numerical results over-estimate the experimental data in terms of load. This is probably due to the difficulties experienced by the developed numerical tool when simulating the stick-slip behavior in crack propagations with local sudden loss of load carrying capability associated to the delamination propagation. In figure 9 the propagation of the delamination, as obtained by running our FE code, is schematically shown on the opening plane by delaminated area (brighter elements) at different load steps. The computed delamination propagation is associated to a sudden decrease of load at the beginning of growth (1.53 mm – 2.55 mm applied displacement) while the load does not vary considerably as the applied displacement increases (2.55 mm – 7.77 mm applied displacement). This behavior is pointed out also in figure 10 where the load is plotted as a function of the crack length. In figure 11 the distribution of G_I along the delamination front at growth initiation is reported. The distribution shows a constant value of G_I, as expected, except for the edges of the specimen, where border effects become relevant and the delamination growth delayed.

3.2 RFI 2-5 MM GAP WIDTH CONFIGURATION

The second analyzed DCB configuration is the RFI "2-5 mm gap width". This configuration allows to investigate the influence of gap width on the overall structural behavior of the DCB specimens. Since the deformed shapes are very similar to the DCB RFI base configuration ones, they will not be shown.

In figure 12, comparisons between numerical and experimental load/applied displacement curves are presented. The agreement between numerical analysis and test is again very good. The delamination growth initiation (load=0.142 kN; applied displacement=1.538 mm) is again predicted very well and the experimental load over-estimation as the delamination growth proceeds, is found to be less relevant with respect to the DCB-RFI base configuration. After the first stick-slip phase, the simulated delamination growth becomes more stable as it can be pointed out analyzing figure 13, where the applied load is plotted as a function of the crack length. The delamination growth evolution and the G_I distribution along the delamination front are very similar to the previously discussed DCB-RFI base configuration; for the sake of brevity, they will not be shown.

3.3 RFI LONG STITCH CONFIGURATION

The third analyzed test-case is the DCB-RFI long stitch configuration. This configuration has been analyzed to investigate the influence of the stitch length on the overall DCB specimen structural behavior. A zoomed view of the deformed shape for an applied displacement of 4.56 mm is presented in figure 14 where the tendency of delamination, to growth first in the middle of the specimen and then at its edges can be clearly appreciated. This trend can also be appreciated in figure 15 where the developed area is shown for some relevant load steps. In figure 16 the numerical and experimental load/applied displacement curves are presented. The agreement between experimental and numerical results is very good considering the scatter in the experimental tests. The overall behavior of the DCB-RFI long stitch configuration, in terms of load/applied displacement curves, is very similar to the two previously analyzed configurations. The growth initiation takes place at 0.139 kN for an applied displacement of 1.44 mm. In figure 17, the load as a function of the crack length is shown. The beginning of the delamination growth seems to be more stable with respect to the previously analyzed DCB-RFI configurations. In figure 18 the G_I distribution is presented. Again the edge effects seem to be more relevant with respect to the other two configurations as demonstrated by the lower G_I values close to the edges.

3.4 RIFT LONG STITCH CONFIGURATION

In order to take into account the influence of the manufacturing process on the structural behavior of DCB NCF specimens, the RIFT long stitch configuration has been analyzed. The deformed shapes for different load steps are shown in figure 19. The experimental and numerical load/applied displacement curves are shown in figure 20. The applied load at delamination growth initiation (0.078 kN) is half the load values found for the DCB-RFI configurations. The behavior of the curve is very similar to the previously analyzed test cases, except for the drop in the load after the beginning of the delamination growth, which is more relevant for the RIFT configuration. The agreement between numerical and experimental results is extremely good in every phase of the delamination growth. Figure 21 shows that the edge effects, also for the DCB RIFT long stitch configuration are relevant; however, they are not as

relevant as the edge effects in the DCB-RFI long stitch configuration. This fact is proved also by the G_{Ic} distribution along the delamination front shown in figure 22 which is not as smooth as in the case of the DCB-RFI long stitch configuration. Finally, some considerations should be introduced about figure 23 showing the applied load as a function of the crack length for the DCB-RIFT "long stitch" configuration. Indeed, the RIFT configuration is characterized by three delamination growth phases. A first very stable phase with a linear functionality of the delamination opening with the applied load; a second stick-slip phase characterized by a sudden drop in the load, and, a last phase, that is substantially stable (as in the RFI configuration) where the applied load reaches a plateau zone.

4.0 CONCLUSIONS

In this paper a novel FEM approach able to simulate the mechanical behavior, including delamination growth, of Non Crimp Fabric Composites is introduced. This approach based on the Stiffness Averaging Method and Modified Virtual Crack Closure Technique has been implemented in the "research oriented" B2000 FE code. A validation campaign has been performed on Double Cantilever Beam specimens focused on the assessment of the effectiveness of the delamination growth approach together with the NCF composite material formulation. The comparisons between numerical results and experimental data have shown an excellent agreement for all the analyzed configurations (RFI, RIFT, long-stitch, 2/5 mm gap-width, base configuration). The implemented FE procedure has been able to predict with good accuracy either initiation loads of the delamination growth and relevant applied displacements. All the configurations present a growth initiation characterized by a stick-slip behavior followed by a stable behavior. The extension of the stick-slip growth phase seems to be dependent especially on the stitch length and on the manufacturing process. Indeed, this growth phase seems to be more extended in the long stitch configurations; in particular the RIFT configuration shows an alternate stable / stick-slip phase. In general, convergence difficulties have been encountered in the delamination growth phase characterized by sudden drop of load. In all the analyzed configurations, the delamination starts to growth in the middle of the width, and then extends to the edges. This effect is more evident in the long stitch configurations and in particular in the RIFT configuration. In conclusion, all the simulations of the

coupon tests proved the good capability of the developed numerical tool to predict the mechanical performances of the NCF composite structures when delamination growth and contact phenomena are involved. However, the numerical tool could be enhanced in order to better predict the drop of load in the delamination growth phase characterized by stick- slip behavior. Furthermore failure criteria for fibers breakage and matrix cracking could be implemented in order to better predict the extension of the damaged areas.

5.0 AKNOWLEDGEMENTS

This work has been performed within the framework FALCOM project – *Failure, Performance and Processsing Prediction for Enfhanced Design with Non-Crimp-Fabric Composites* -. FALCOM is an RTD project, partially funded by the European Union, Contract N° G4RD-CT-2001-00694.

A particular Acknowledgement is due to Jens Baaran for the experimental activity on Mode I fracture toughness of NCF composite samples, which allowed us to validate our model.

REFERENCES

[1] Dexter H. B., Hasko G. H., "Mechanical Properties of Multiaxial Warp-Knit Composites", Composite Science and Technology, Vol. 56, pp 367-380, 1996.

[2] Zhang, Y., Huang, Z,-M, Ramakrishna, S., "Tensile Behaviour of Multilayered Knitted Fabric Composites with Different Stacking Configuration", Applied Composite Materials, Vol. 8 N° 4, pp. 279-295, 2001.

[3] Byun, J.-H., Chou, T.-W., "Modelling and Characterisation of Textile Structural Composites. A. Review", Journal of Strain Analysis for Engineering Design, Vol. 24 N° 4, pp. 253-262, 1989.

[4] Pastore A. C. M., Whyte D. W., Soebruto H., Ko F. K., "Design and Analysis of Multiaxial Warp Knit Fabrics for Composites", Int. Journal of Industrial Fabrics, Vol. 5 N° 1, pp. 4-17, 1986.

[5] Drapier S., Wisnom M. R., "Finite-element investigation of the compressive strength of non-crimp-fabric based composites", Composite Science and Technology, vol. 59 N°8, pp. 1287-1297, 1999.

[6] Drapier S., Wisnom M. R., "A finite-element investigation of the interlaminar shear behaviour of non-crimp-fabric-based composites", Composite Science and Technology, Vol. 59 N°16, pp: 2351-2362, 1999.

[7] Ramakrishna, S. and Hull, D., "Tensile Behaviour of Knitted Carbon-Fiber Fabric/Epoxy Laminates, part II: Prediction of Tensile Properties". Composite Science and Technology, vol. 50 , N°2, pp:249-258, 1994.

[8] Ramakrishna, S. and Hull, D., "Tensile Behaviour of Knitted Carbon-Fiber Fabric/Epoxy Laminates, part II: Experimental". Composite Science and Technology, vol. 50 , N°2, pp:237-247, 1994.

[9] Ramakrishna, S., "Analysis and Modelling of Plain Weft knitted-fabric Reinforced Composites". Jounal of Composite Materials, Vol. 31, N°1 pp.52-70, 1997.

[10] Ishikawa, T., Chou, T.W., "Stiffness and Strength Behaviour of woven Fabric Composites". Jounal of Materials Science, Vol. 71, N°11 pp.3211-3220, 1982.

[11] Edgren, F., Asp, L.E., "Approximate Analytical Constitutive Model for Non-Crimp Fabric Composites". Composites Part A: Applied Science and Manufacturing, Vol. 36, N°2 pp.173-181, 2005.

[12] Pastore C. M. and Gowayed Y. A., "A self-consistent fabric geometry model: modification and application of a fabric geometry model to predict the elastic properties of textile composites", Journal of Composites Technology & Research, JCTRER, Vol. 16, No. 1, pp. 32-36, 1994.

[13] Edgren, F., Mattsson, D., Asp, L.E., Varna, J., "Formation of Damage and Its Effects on Non-Crimp Fabric Reinforced Composites Loaded in Tension", Composites Science and Technology, Vol. 64, No. 5, pp. 675-692, 2004.

[14] Edgren, F., Asp, L.E., Joffe, R., "Failure of NCF Composites subjected to Combined Compresion and Shear Loading", Composites Science and Technology, Vol. 66 No. 15, pp. 2865-2877, 2006.

[15] K. A. Dransfield, L. K. Jain and Y. W. Mai. "On the Effects of Stitching in CFRPs – I. Mode I Delamination Toughness". Composite Science and Technology, Vol. 58, pp.815-828, 1998.

[16] K. A. Dransfield, L. K. Jain and Y. W. Mai. "On the Effects of Stitching in CFRPs – II. Mode II Delamination Toughness". Composite Science and Technology, Vol. 58, pp.829-837, 1998.

[17] Xiaoping Ruan and Tsu-Wei Chou, "Failure Behaviour of Knitted Fabric Composites", Journal of Composite Materials, Vol. 32, No. 3, pp.198-222, 1998.

[18] Tessitore, N., Riccio, A., "A novel FEM model for biaxial non-crimp fabric composite materials under tension", Computers & Structures, Vol. 84 N°(19-20), pp. 1200-1207, 2006.

[19] Tada H., Paris P. C. and Irwin G. R., "Stress Analysis of Cracks Handbook". Del. Research Corp, 1985

[20] Chou T. and Ko F. K., "Textile Structural Composites", Elsevier, 1989.

[21] Bogdanovich A. E. and Pastore C. M., "Mechanics of Textile and Laminated Composites", Chapman & Hall, First Edition, 1996.

[22] Jens Baaran ," DLR structural element definition and test plan", Nov 2004, FALCOM/WP3/DLR TECH0003

[23] FALCOM Technical Annex – Project Programme, Dec 2002, FALCOM/WP1/QQ/PM002

	Hexcel M36	Hexcel RTM6
E (Gpa)	3.5	2.89
G (Gpa)	1.23	1.017
ν	0.42	0.42
V_m	0.4	0.3

Table 1: Material properties of matrix – DCB test-case

Tow	
E_1 (Gpa)	237
$E_2=E_3$ (Gpa)	20
$G_{12}=G_{13}=G_{23}$ (Gpa)	13
$\nu_{12}=\nu_{13}=\nu_{23}$	0.22
V_f	0.85
Tow thickness (mm)	0.25
c/2 (mm)	0.12

Table 2: Material properties and geometrical characteristic of fiber tows – DCB test-case

	Sinterama Zerbion		
	Long stitch	2-5 mm gap width	base
E_1 (Gpa)	61	61	61
$E_2=E_3$ (Gpa)	4.2	4.2	4.2
$G_{12}=G_{13}=G_{23}$ (Gpa)	2.9	2.9	2.9
$\nu_{12}=\nu_{13}=\nu_{23}$	0.29	0.29	0.29
A (mm^2)	0.006	0.006	0.006
S_{gauge} (mm)	4.0	5.0	1.5
S_{len} (mm)	4.0	2.5	2.5
θ_{stitch} (deg)	35°	35°	35°

Table 3: Material properties of stitching thread and stitching parameters – DCB test-case

	RFI			RIFT
	Base	Long stitch	2-5 mm gap width	Long stitch
$G_{Ic}(J/m^2)$	564	579.8	604.4	472

Table 4: Mode I Critical Energy Release Rate for all the analyzed DCB test-cases

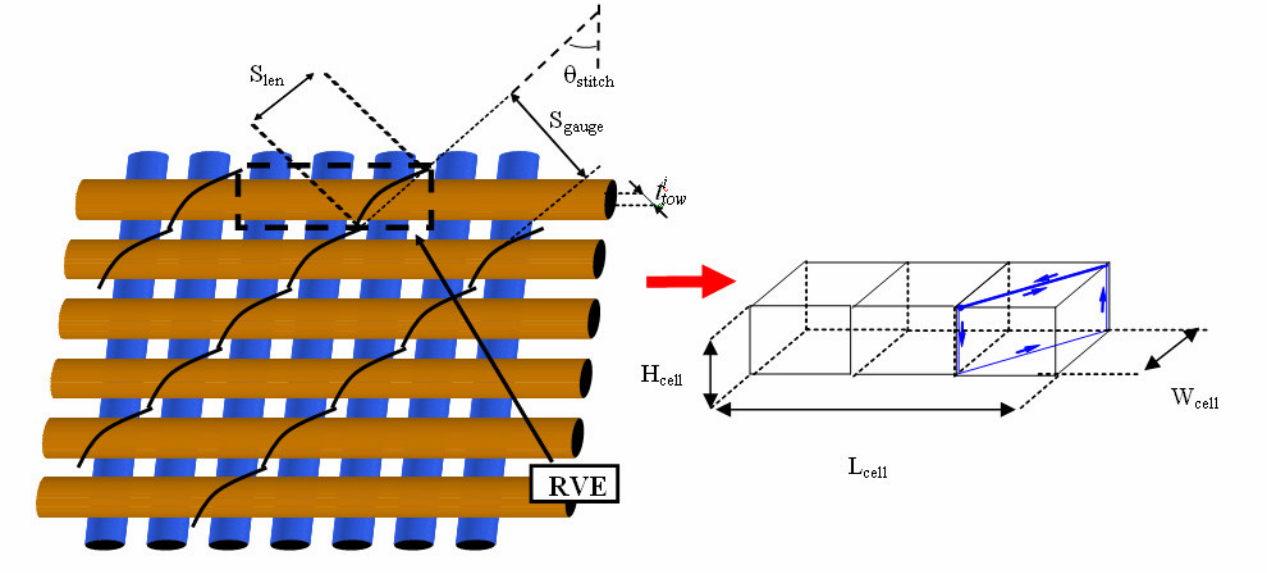

Figure 1: Example of RVE for a biaxial perform with chain stitch pattern

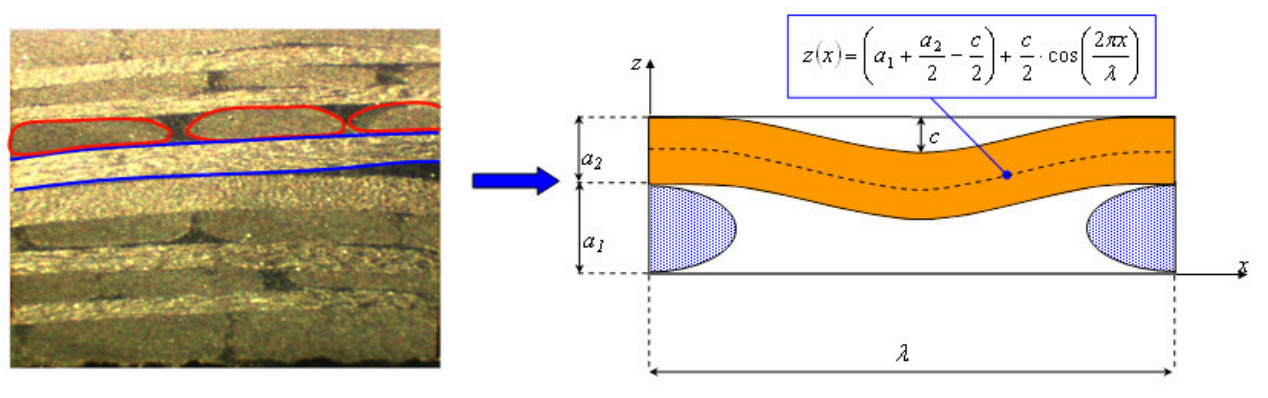

Figure 2: Waviness of bundles in the RVE for a biaxial perform

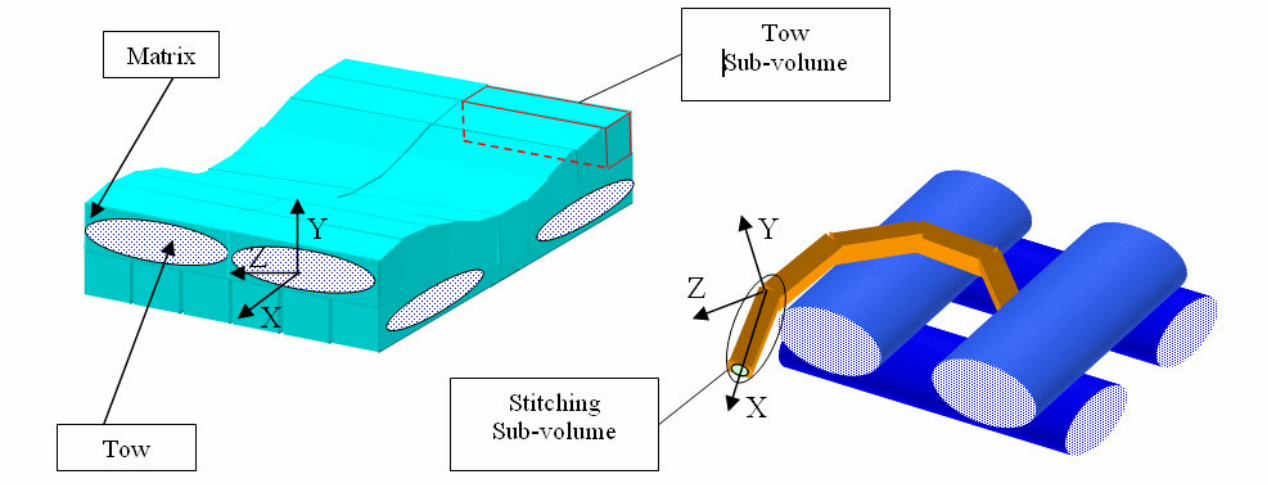

Figure 3: Tows and stitching sub-volumes representation

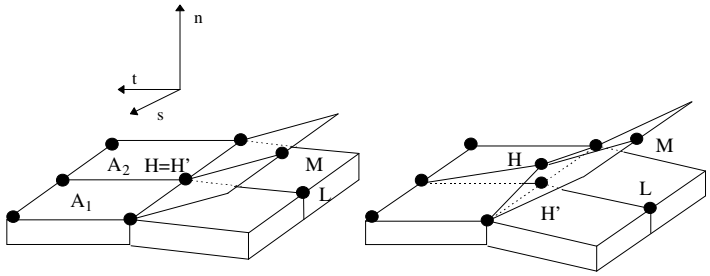

a) Interface Fracture element activated

b) Interface Fracture element released

Figure 4: Interface fracture element

Long Stitch:
S_{len} = 4 mm;
S_{gauge} = 4 mm;
θ_{stitch} = 35°;
L_{cell} =4.88 mm
W_{cell} =3.22 mm

2.5 mm gauge width:
S_{len} = 4 mm;
S_{gauge} = 2.5 mm;
θ_{stitch} = 35°;
L_{cell} =3.05 mm
W_{cell} =3.22 mm

Base:
S_{len} = 2.5 mm;
S_{gauge} = 1.5 mm;
θ_{stitch} = 35°;
L_{cell} =1.8 mm
W_{cell} =2.04 mm

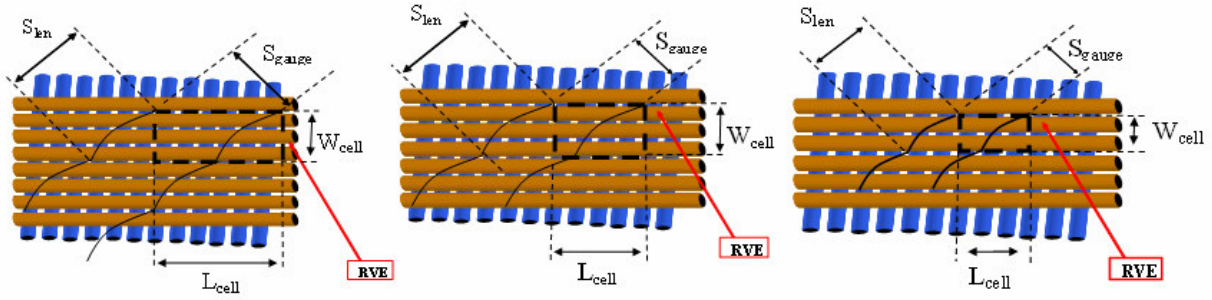

Figure 5: Repetitive Volume Elements Geometrical dimensions for the analyzed RFI configurations

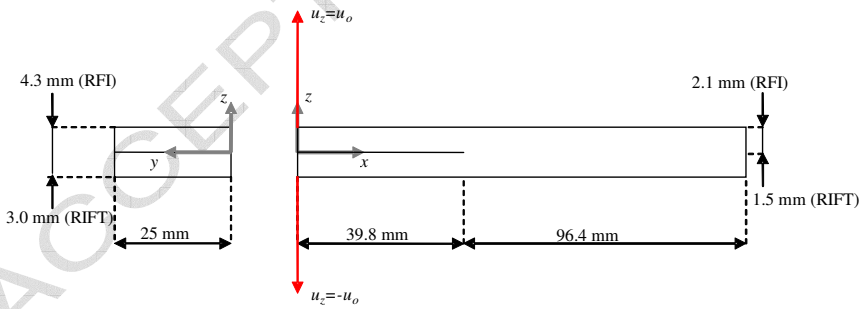

Figure 6: Geometrical dimensions and boundary conditions of DCB specimens

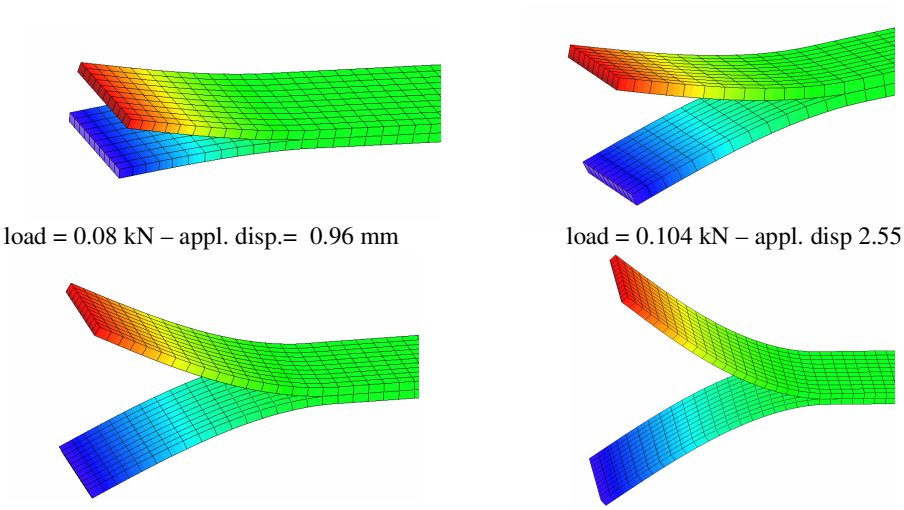

Figure 7: Deformed shapes (ampl. 5) DCB-RFI-base configuration at different steps during the loading process

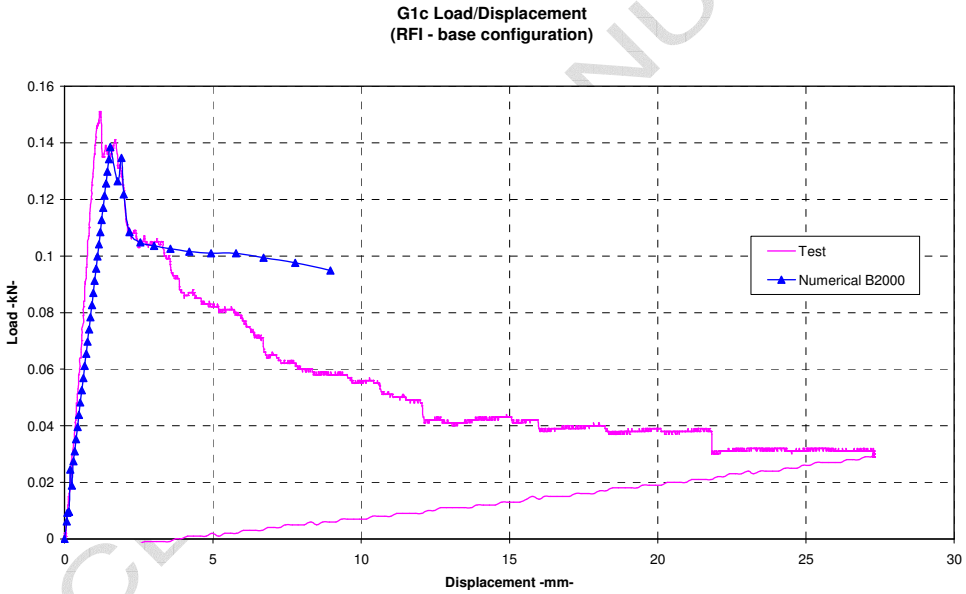

Figure 8: Load/displacement curve – DCB RFI base configuration – comparison against experimental results

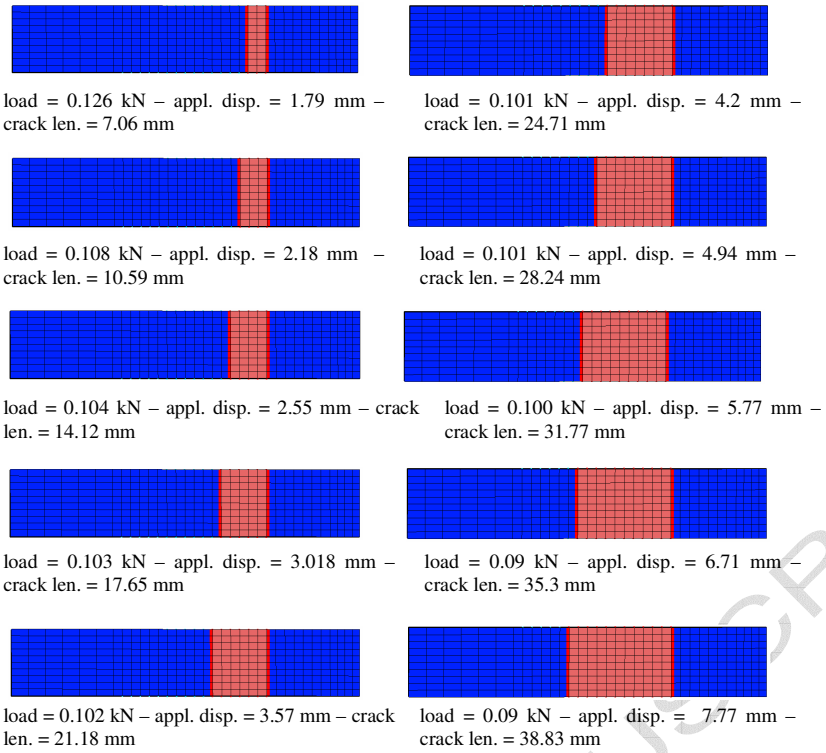

Figure 9: Delamination propagation during loading process – DCB RFI base configuration

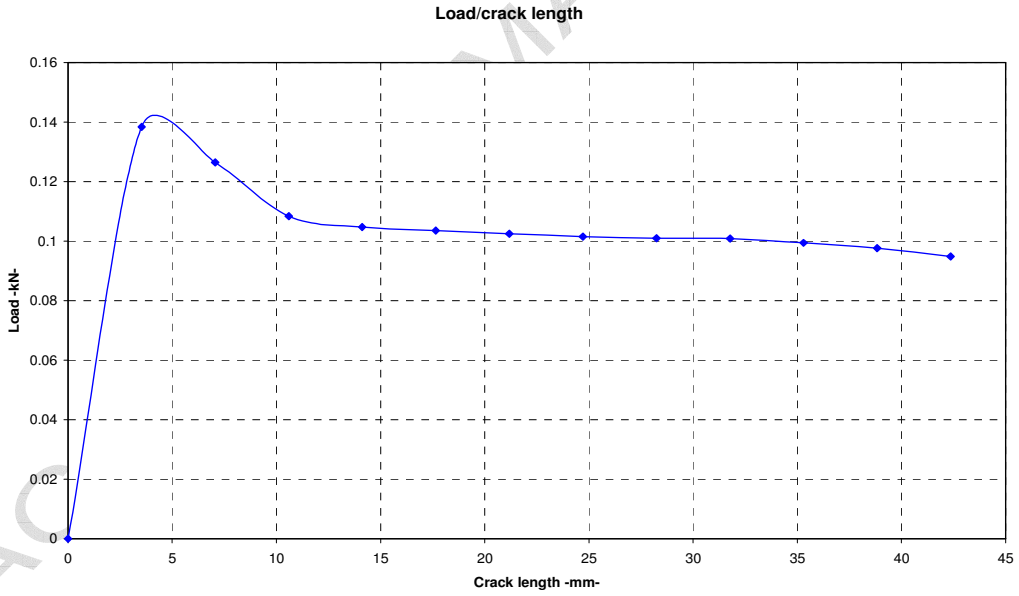

Figure 10: Load as a function of the crack length – DCB RFI base configuration

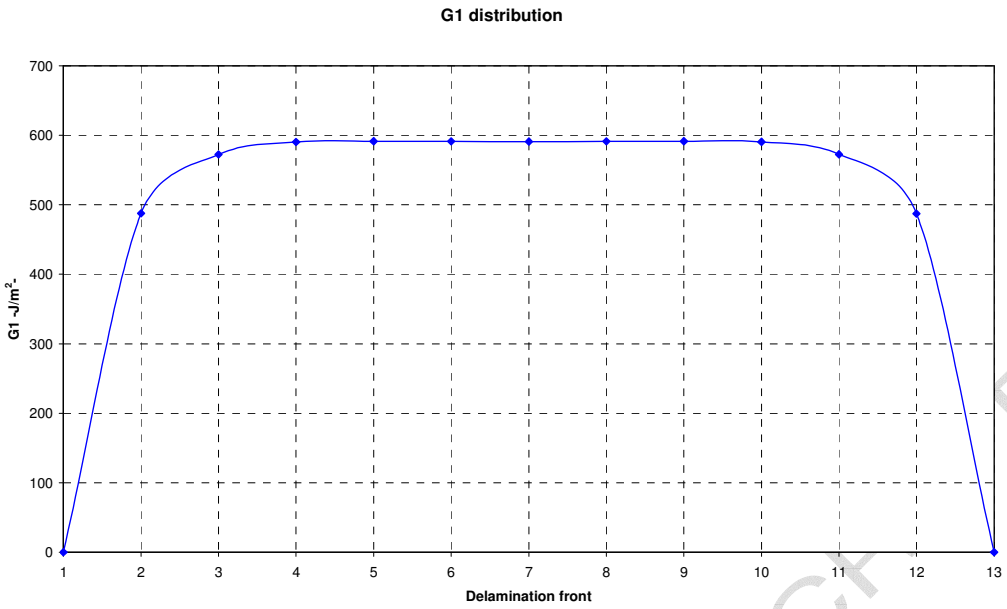

Figure 11: GI distribution at delamination front – DCB RFI base configuration

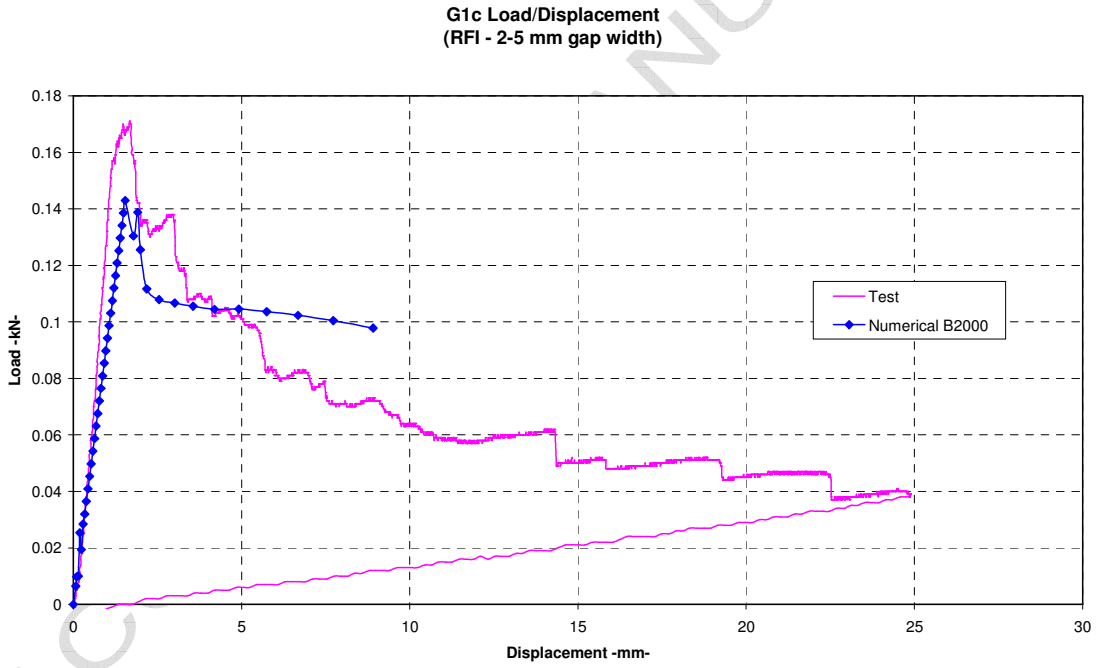

Figure 12 Load/applied displacement curve – DCB RFI 2-5 mm gap width configuration - Comparison between numerical results and experimental data

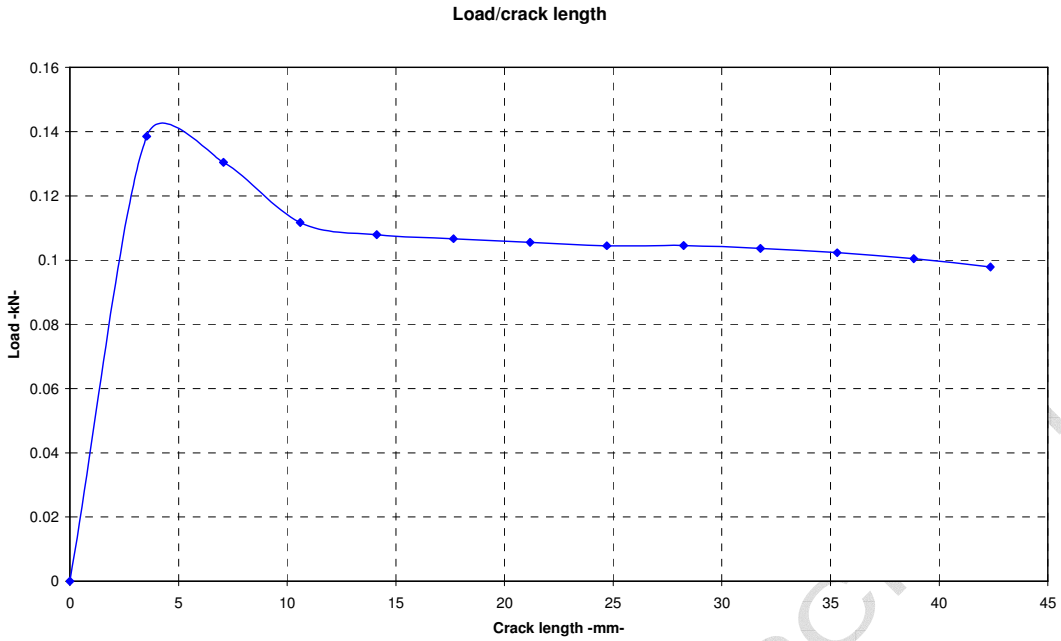

Figure 13: Load as a function of the crack length – DCB RFI 2-5 mm gap width configuration

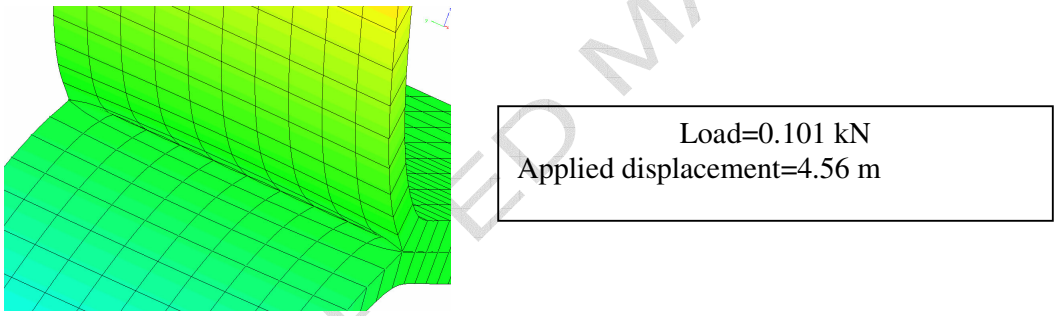

Figure 14: Zoom-in of the deformed shape – DCB RFI long stitch configuration

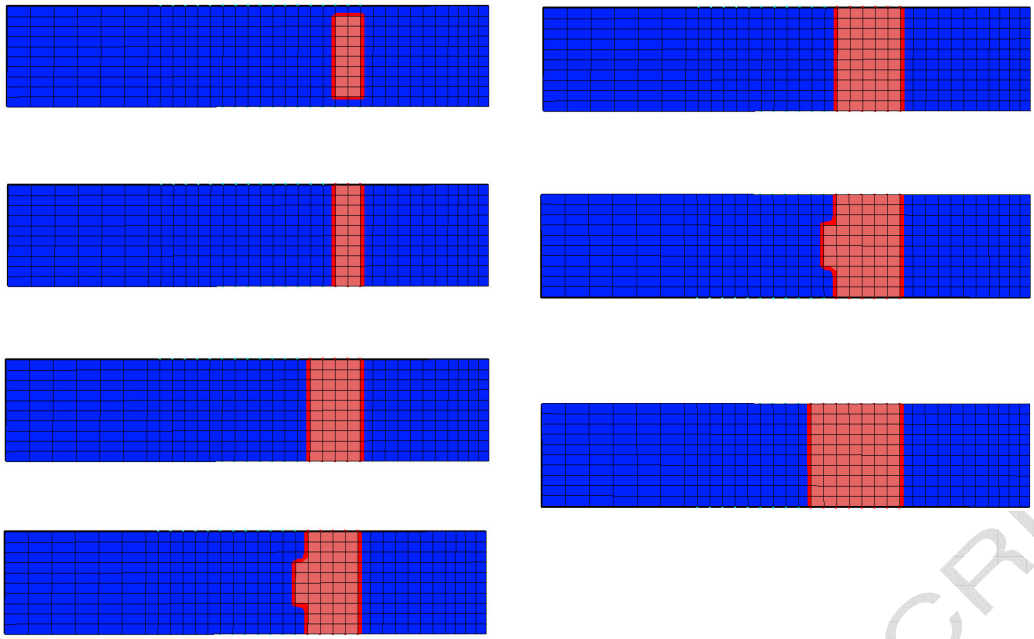

Figure 15: Delamination propagation during loading process of a DCB RFI long stitch configuration model

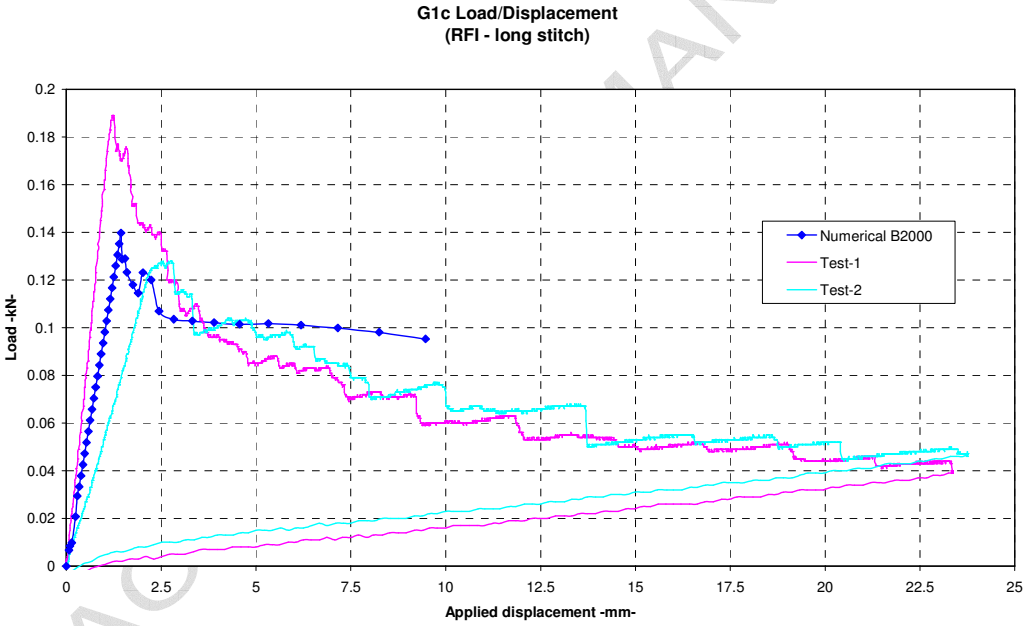

Figure 16: Load vs. applied displacements – DCB RFI long stitch configuration – Comparison between numerical results and experimental data

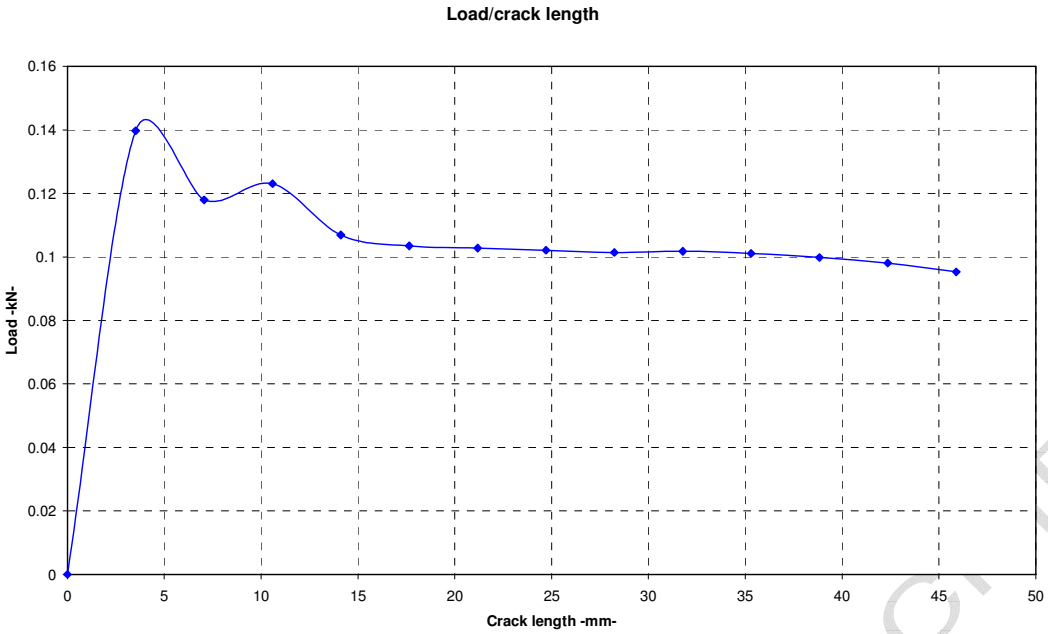

Figure 17: Load vs. crack length for a DCB RFI long stitch configuration sample

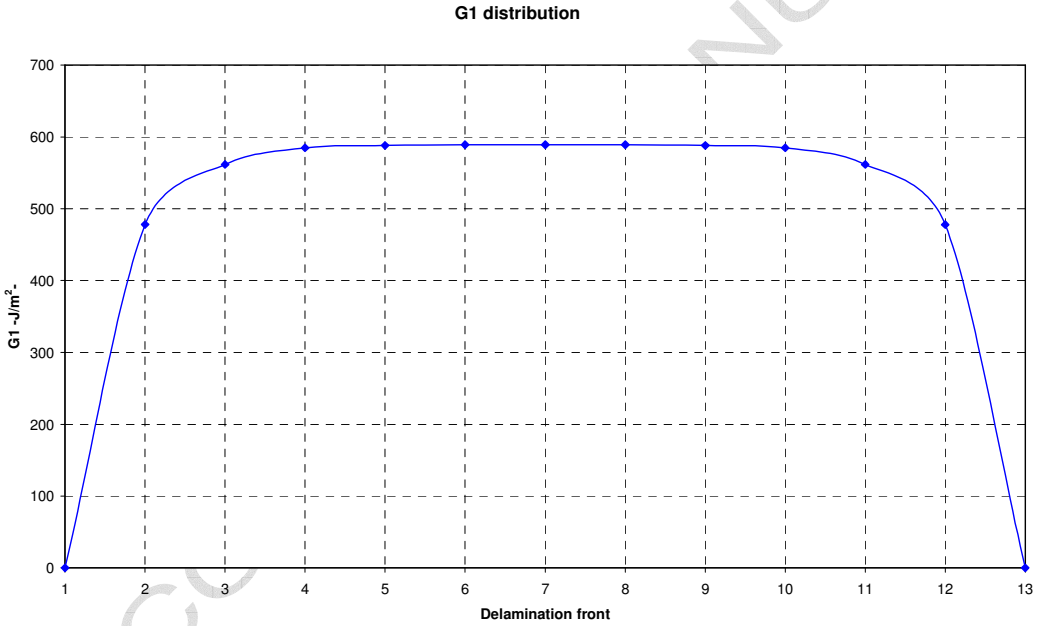

Figure 18: G_I distribution along the delamination front for a DCB RFI long stitch configuration sample

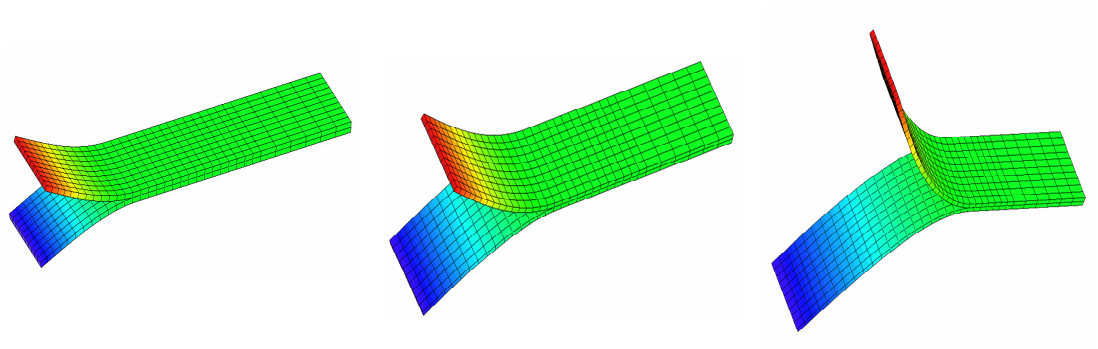

Figure 19: Deformed shapes at different load steps (ampl. 5) for a DCB RIFT long stitch configuration model

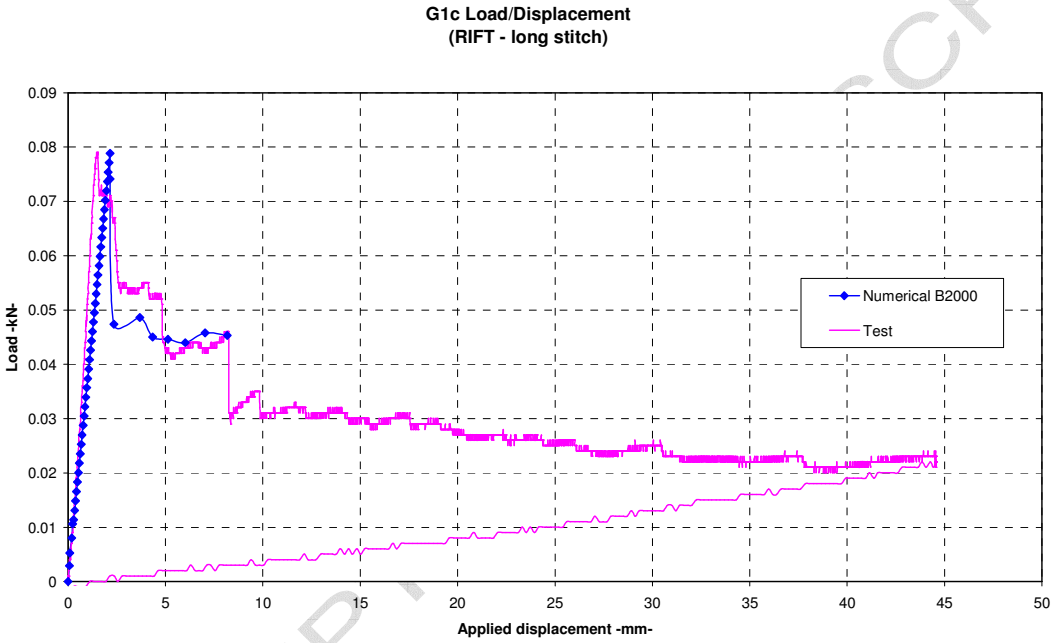

Figure 20: Comparison between numerical results and experimental data of load vs. applied displacement for DCB RIFT long stitch configuration sample.

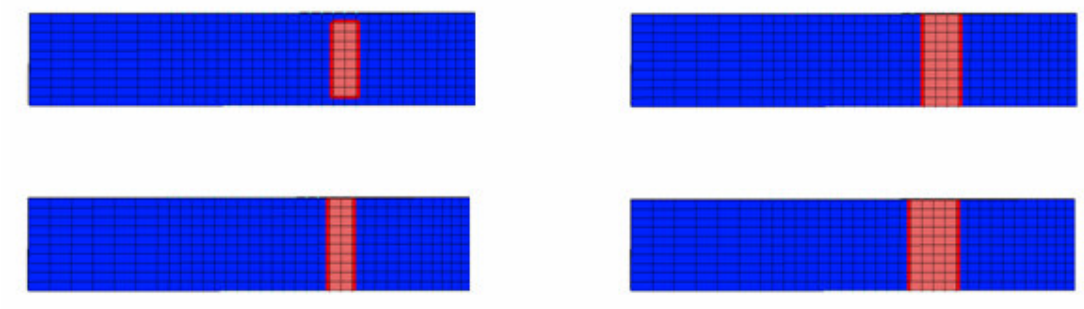

Figure 21: Delamination propagation during loading process for a DCB RIFT long stitch configuration sample.

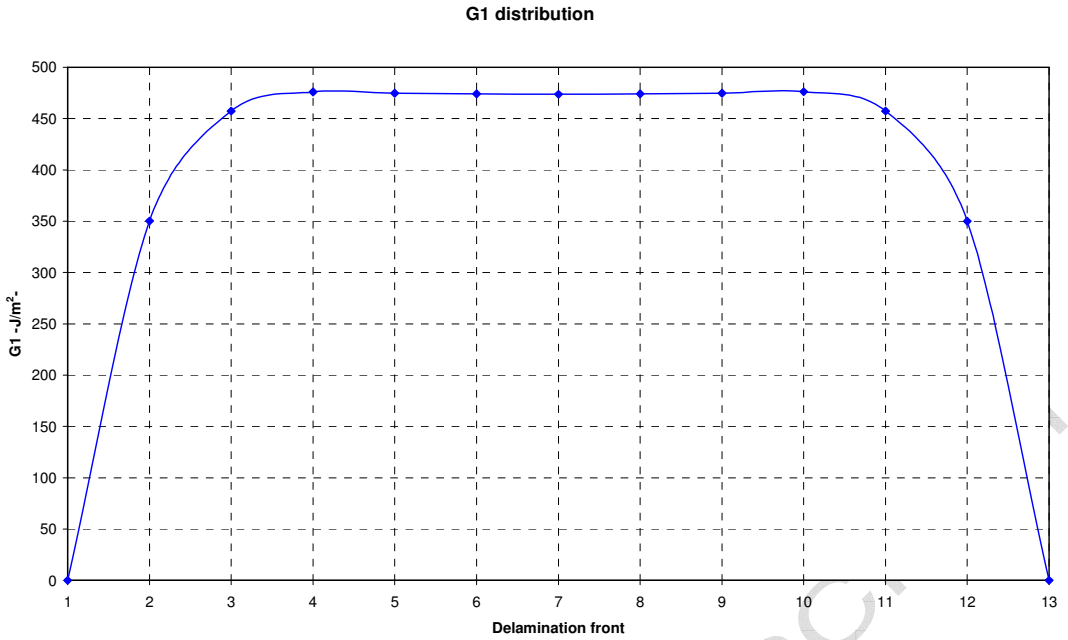

Figure 22: G_I distribution along delamination front for a DCB RIFT long stitch configuration sample

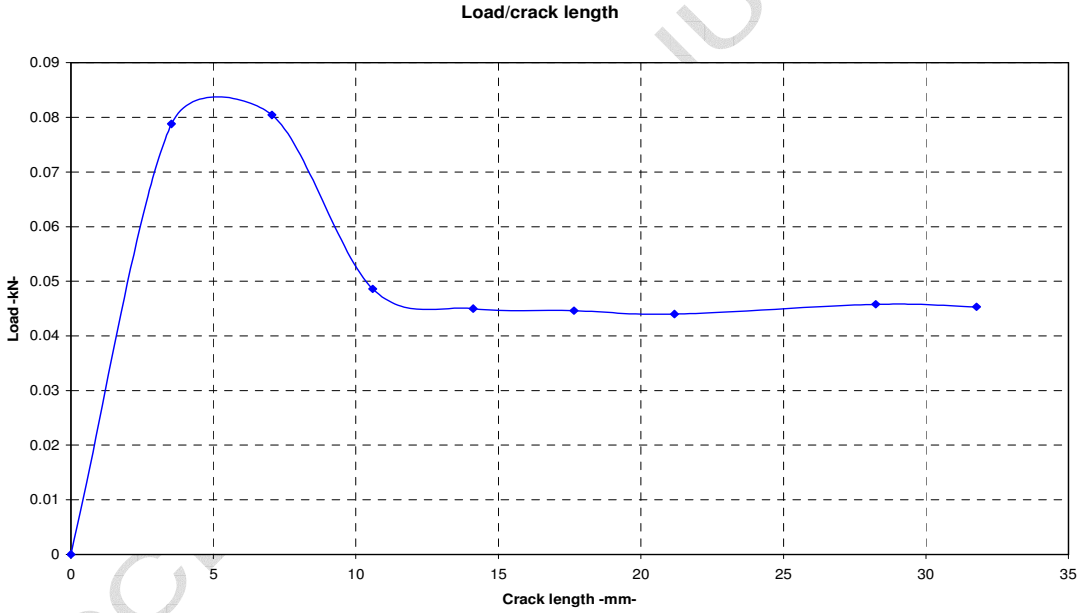

Figure 23: Applied load as a function of the crack length – DCB RIFT long stitch configuration